Subtlety of modes trapped by vortices in a topological superconducting heterostructure

Xin-Hai Tu,[1,2] Xian-Gang Wan,[1,2] and Ning Hao[3,*]

[1]*National Laboratory of Solid State Microstructures and School of Physics, Nanjing University, Nanjing 210093, China*

[2]*Collaborative Innovation Center of Advanced Microstructures, Nanjing University, Nanjing 210093, China*

[3]*Anhui Province Key Laboratory of Low-Energy Quantum Materials and Devices, High Magnetic Field Laboratory, HFIPS, Chinese Academy of Sciences, Hefei, Anhui 230031, China*

(Received 3 January 2024; revised 27 March 2024; accepted 28 March 2024; published 10 April 2024)

In a topological superconducting heterostructure comprising an *s*-wave superconductor and a semiconductor with Rashba spin-orbit coupling, several distinct modes emerge when an external magnetic field is applied: Majorana zero-energy modes, trivial Caroli–de Gennes–Matricon modes, and edge modes. We find three subtle properties of the modes under the fine tuning of the external magnetic field and Rashba spin-orbit coupling. (1) The spatial configuration of Majorana zero-energy modes undergoes a dramatic change when flipping the direction of magnetic field. (2) In the topological nontrivial regime, the Caroli–de Gennes–Matricon modes and edge modes exhibit spatial oscillatory behavior across the entire sample scale and approach zero energy as the strength of the Rashba spin-orbit coupling decreases. (3) In the topological trivial regime, another type of zero-energy mode may also manifest at the vortex center. The key distinction from the Majorana zero-energy mode is its lack of spatial coherence and no coexistence of edge modes. These properties highlight the modes' sensitivity to the tuning parameters and impose constraints on the experimental determination of Majorana zero-energy modes.

DOI: 10.1103/PhysRevB.109.144512

I. INTRODUCTION

The realization of topological superconductivity, a crucial avenue for the topological quantum computation [1–3], has been proposed in various schemes. Intrinsic *p*-wave superconductors, such as Sr_2RuO_4 [4], naturally offer a platform for hosting Majorana zero-energy modes, which are their own antiparticles and obey non-Abelian braiding statistics [5,6]. However, the stringent experimental conditions and the rarity of natural *p*-wave superconductors has limited progress in this field. Recent advancements have been made based on the Fu-Kane theory [7]. The semiconductor with Rashba spin-orbit coupling or topological surface states contacting to an *s*-wave superconductor via the superconducting proximity effect mimics a spinless $p + ip$ superconductor. Notable examples include Rashba semiconductor InSb/Nb nanowires [8,9], the topological insulator $Bi_2Te_3/NbSe_2$ [10,11], and the topological crystalline insulator $Sn_{1-x}In_xTe$ [12–15]. Furthermore, Majorana zero-energy modes (MZMs) have also been demonstrated to exist in superconducting vortices [16–19]. The presence or absence of a second-order kinetic term gives rise to completely opposite topological parameter regions, depending on whether an odd or even number of Fermi surfaces is involved.

In general, the presence of MZM within a vortex is often accompanied by several other types of modes, namely, edge modes (EMs), Caroli–de Gennes–Matricon modes (CdGMMs) [20,21], and vortex core modes (VCMs). We call all trivial bound states located in the vortex core center VCMs. CdGMMs are peaked at the place $r_C \approx |n|/k_F$ from the vortex core center with their energy estimated to be $E_C \approx n\Delta^2/E_F$, where n, k_F, E_F, and Δ are the nonzero half-integer/integer angular momentum, the Fermi velocity, the Fermi energy, and the superconducting order parameter, respectively. In the presence of disorder or external fields, CdGMMs may also emerge with zero energy [22–24], which can introduce obstructions when experimentally trying to identify MZMs.

In this paper we undertake a numerical investigation of the Bogoliubov–de Gennes (BdG) equation within the context of a fully gapped Rashba spin-orbital coupling (SOC) *s*-wave superconductor, featuring Zeeman splitting induced either through an external magnetic field or contact with a magnetic insulator. We explore the localization of MZMs within the vortex, revealing that they are not exclusively peaked at the vortex center. Of particular interest is the dominance of spin-down components of MZMs characterized by angular momentum $l = \pm 1$, a behavior that emerges when the direction of the Zeeman field (ZF) is inverted relative to the chirality of momentum ($p_\pm = |p|e^{\pm i\theta_p}$). Then the spatial distribution of these MZMs closely resembles that of CdGMMs. In the topological nontrivial regime, we find CdGMMs and EMs exhibit spatial oscillatory behavior across the entire sample scale and approach zero energy as the strength of the SOC decreases. In the topological trivial regime, the trivial zero-energy VCMs emerge when the SOC is weak. To experimentally verify MZMs and VCMs, the spatial coherence and coexistence of EMs can be checked. The structure of this paper is organized as follows. In Sec. II we introduce the theoretical model. In Sec. III we present detailed numerical

*haon@hmfl.ac.cn

results along with straightforward explanations of the various aforementioned novel phenomena. In Sec. IV we delve into discussions and present our conclusions.

II. THEORETICAL MODEL

For a type-II superconductor, if the magnitude of the magnetic field is significantly smaller than the upper critical field, denoted as $H \ll H_{c2}$, a condition where the separation between distinct vortices greatly exceeds the coherence length ξ, and the effective Zeeman effect is much larger than the orbital effect for the experimental platform with large effective g factor ~ -200 [25], we can safely neglect the direct coupling of electrons to the magnetic field in the kinetic energy term [20]. Consequently, we can formulate the single-particle effective Hamiltonian for the conduction bands of a Rashba SOC type-II superconductor at temperatures above the superconducting transition temperature under the influence of a magnetic field. Hereafter, we adopt $\hbar = 1$ for simplicity, and the Hamiltonian is given by

$$H_0 = \frac{p^2}{2m^*} - \mu + \alpha(\sigma_x p_y - \sigma_y p_x) + B_z \sigma_z. \tag{1}$$

Here, m^* represents the effective mass of a conduction-band electron, μ is the chemical potential, α characterizes the strength of the Rashba SOC, known for its spin-momentum locking properties [26,27], B_z denotes the effective Zeeman coupling due to the magnetic field along the z direction, and σ represents the Pauli matrix for spin. This model closely resembles that of the conduction band of a semiconductor with SOC interfacing with a magnetic insulator [17,28]. Notably, due to the presence of the kinetic energy term, two spin-orbit-split Fermi surfaces emerge, distinguishing it from the model of Dirac surface states in a topological insulator, where an odd number of bands cross the Fermi level [7]. If we eliminate the spin-momentum locking term, i.e., by replacing $(\sigma_x p_y - \sigma_y p_x)$ with $(\sigma_x p_y + \sigma_y p_x)$, or by reversing the direction of the Zeeman field, the spin and position of MZMs within the vortex become distinct, as shown later.

The corresponding BdG equations, formulated within the Nambu space representation $\{c_\uparrow, c_\downarrow, c_\downarrow^\dagger, -c_\uparrow^\dagger\}^T$ below the superconducting transition temperature, can be expressed as

$$\begin{pmatrix} H_0 & \Delta_s(\mathbf{r}) \\ \Delta_s^\dagger(\mathbf{r}) & -\sigma_y H_0^* \sigma_y \end{pmatrix} \Phi(\mathbf{r}) = E\,\Phi(\mathbf{r}). \tag{2}$$

Here, $\Phi(\mathbf{r}) = [u_\uparrow(\mathbf{r}), u_\downarrow(\mathbf{r}), v_\downarrow(\mathbf{r}), -v_\uparrow(\mathbf{r})]^T$ represents the quasiparticle wave function. It is worth noting that there exists a band gap within the bulk until the topological critical condition $B_z^2 = \Delta_s^2 + \mu^2$ is satisfied [17,28–30]. MZMs emerge within the vortex in the topological parameter regime where $B_z^2 > \Delta_s^2 + \mu^2$. If the spin-diagonal kinetic energy term is absent, the topological condition reverses [17,28]. This system exhibits a preservation of spin-orbit-pseudospin rotation symmetry, and the BdG Hamiltonian commutes with the operator $J_z = L_z + \frac{1}{2}(\sigma_z - \tau_z)$, where L_z signifies the z component of orbital angular momentum, and τ is the Pauli matrix in Nambu space. Consequently, the BdG equations can be decoupled into different angular momentum channels, with the corresponding spinor wave function expressed as

$$\Phi(\mathbf{r}) = e^{il\theta}[u_\uparrow^l(\mathbf{r}), u_\downarrow^{l+1}(\mathbf{r})e^{i\theta}, v_\downarrow^{l-1}(\mathbf{r})e^{-i\theta}, -v_\uparrow^l(\mathbf{r})]^T. \tag{3}$$

Given that the BdG equations adhere to particle-hole symmetry, a nondegenerate zero-energy solution can only exist in the $l = 0$ angular momentum channel. Nonetheless, nonzero-angular-momentum contributions from the spin-down components of MZM ($u_\downarrow^1$, $v_\downarrow^{-1}$) do influence the spatial configuration of MZM.

III. NUMERICAL RESULTS AND ANALYSIS

For the sake of computational simplicity, we adopt a two-dimensional circular geometry with a hard wall located at a radius $r = R$. Within this setup, a single vortex is situated at the center, precisely at $r = 0$. In the experimental terms, one can envision R as half the distance separating adjacent vortices. Within the vortex, the superconducting order parameter assumes the following form: $\Delta_s(r, \theta) = \Delta \tanh(r/\xi)e^{i\nu\theta}$, where ξ denotes the coherence length, and ν represents the vorticity of the vortex. To solve the radial BdG equations numerically, we employ an expansion of the spinor wave function in terms of a set of orthogonal normalized bases denoted as $\phi_{lj}(r) = \sqrt{2}J_l(a_{lj}r/R)/[RJ_{l+1}(a_{lj})]$, where J_l signifies the lth-order Bessel function, and a_{lj} corresponds to the jth zero of J_l. These bases automatically satisfy the boundary conditions, specifically, $\phi_{lj}(R) = 0$. Consequently, the radial BdG equations can be reduced to the following form:

$$\begin{pmatrix} T_l^+ & S_l & \Delta_l & 0 \\ S_l^\dagger & T_{l+1}^- & 0 & \Delta_{l+1} \\ \Delta_l^\dagger & 0 & -T_{l-1}^- & -S_{l-1} \\ 0 & \Delta_{l+1}^\dagger & -S_{l-1}^\dagger & -T_l^+ \end{pmatrix} \begin{pmatrix} u_{n\uparrow}^l \\ u_{n\downarrow}^{l+1} \\ v_{n\downarrow}^{l-1} \\ -v_{n\uparrow}^l \end{pmatrix} = E_{nl} \begin{pmatrix} u_{n\uparrow}^l \\ u_{n\downarrow}^{l+1} \\ v_{n\downarrow}^{l-1} \\ -v_{n\uparrow}^l \end{pmatrix}$$

$$(T_l^\pm)_{ij} = \left(a_{lj}^2/2m^*R^2 \pm B_z - \mu\right)\delta_{ij},$$

$$(S_l)_{ij} = \alpha \int_0^R r\phi_{li}^*(r)(\partial_r + \frac{l+1}{r})\phi_{l+1\,j}(r)dr,$$

$$(\Delta_l)_{ij} = \int_0^R r\Delta \tanh(r/\xi)\phi_{li}^*(r)\phi_{l-1\,j}(r)dr. \tag{4}$$

Henceforth, unless otherwise specified, we adopt the following parameter values: $m^* = 0.5$, $\mu = 0$, $\alpha = 0.5$, $\Delta = 0.1$, $\nu = 1$, $\xi = 1$, and $R = j_{\max} = 80$.

A. Majorana zero modes

In Fig. 1 we present plots of the quasiparticle energy across various angular momentum channels, along with the corresponding probability density $|\Phi|^2 = |u_\uparrow|^2 + |u_\downarrow|^2 + |v_\downarrow|^2 + |v_\uparrow|^2$. Notably, a distinct MZM manifests itself exclusively in the $l = 0$ channel. What is intriguing is that the positions of MZMs exhibit marked disparities depending on the direction of the applied ZF. Under negative ZF, a MZM resides precisely at the core center of the vortex, while under positive ZF, the MZM encircles the core. More intriguingly, the strength of the SOC can adjust the position of the second MZM. As SOC strength increases, the second MZM moves closer to the vortex center, mirroring the behavior of the first MZM. To elucidate this off-center phenomenon, we consider

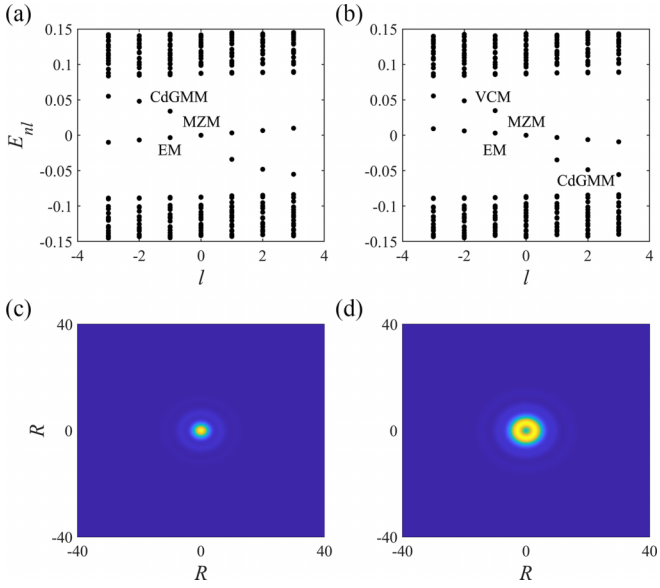

FIG. 1. (a), (b) The quasiparticle energy at different angular momentum channels from −3 to 3, and (c), (d) density of probability of MZMs under different ZFs, (a), (c) $B_z = -0.2$ and (b), (d) $B_z = 0.2$.

the scenario where ZF is sufficiently large, rendering SOC and superconductivity negligible. In this case the BdG matrix becomes diagonal and spin essentially becomes a well-defined quantum number, leading to spin-angular-momentum locking. Simultaneously, the position becomes intertwined with angular momentum. Notice that the zero-energy solution exists only when $T_0^+ = a_{0j}^2/R^2 + B_z = 0$ for negative ZF or $T_1^- = a_{1j}^2/R^2 - B_z = 0$ for position ZF. Obviously, these two cases lead to different contributions from angular momentum and spin $(u_\uparrow^0, u_\downarrow^1)$. As the strength of the SOC increases, leading to enhanced coupling between spin-up and spin-down components of MZM, there is a notable consequence: the component of spin-up in the second MZM becomes more pronounced. Consequently, this results in a greater localization of the MZM at the very center of the vortex core. It is noteworthy that the existence of zero-energy solutions is contingent upon specific values of ZF (as seen in Fig. 4). This phenomenon is indeed a finite-size effect, a subject that has been extensively discussed [29]. In sufficiently small materials, the zero-energy modes may be quenched in finite-size systems due to the interplay between the two edges [31]. However, the off-center effect we observed stems from the kinetic energy term rather than finite-size considerations.

B. Edge modes and CdGM modes

In addition to the MZM, we observe the appearance of two different kinds of modes with discrete energy known as EMs and CdGMMs in nonzero-angular-momentum channels under the influence of negative ZF, as depicted in Fig. 2. The gap between these two kinds of modes can be finely tuned by adjusting the strength of the SOC. When the SOC is sufficiently weak, EMs and CdGMMs become degenerate, and the EMs seamlessly evolve into CdGMMs. In the case of positive ZF, a similar situation arises but with one distinction: the state with higher energy corresponds to VCMs instead of CdGMMs in the $|l| = 1$ channel, as shown in Fig. 3. This discrepancy can be attributed to the differential contributions of angular momentum, akin to what we observed in the case of MZMs. Notably, the presence of a minigap between the VCMs and MZMs plays a vital role in shielding the MZMs from the adverse effects of finite temperature and disorder. Hence, the magnitude of this minigap holds paramount significance in

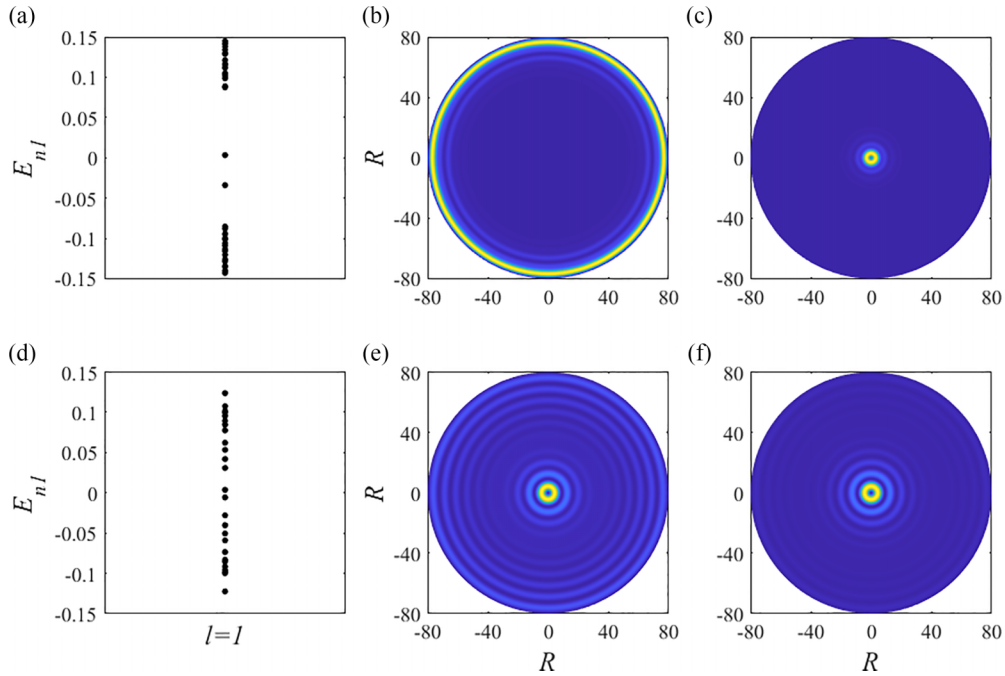

FIG. 2. (a), (d) The quasiparticle energy and density of possibility of (b), (e) EM and (c), (f) CdGMM at $l = 1$ channel under negative ZF $B_z = -0.2$ with (a)–(c) $\alpha = 0.5$ and (d)–(f) $\alpha = 0.1$.

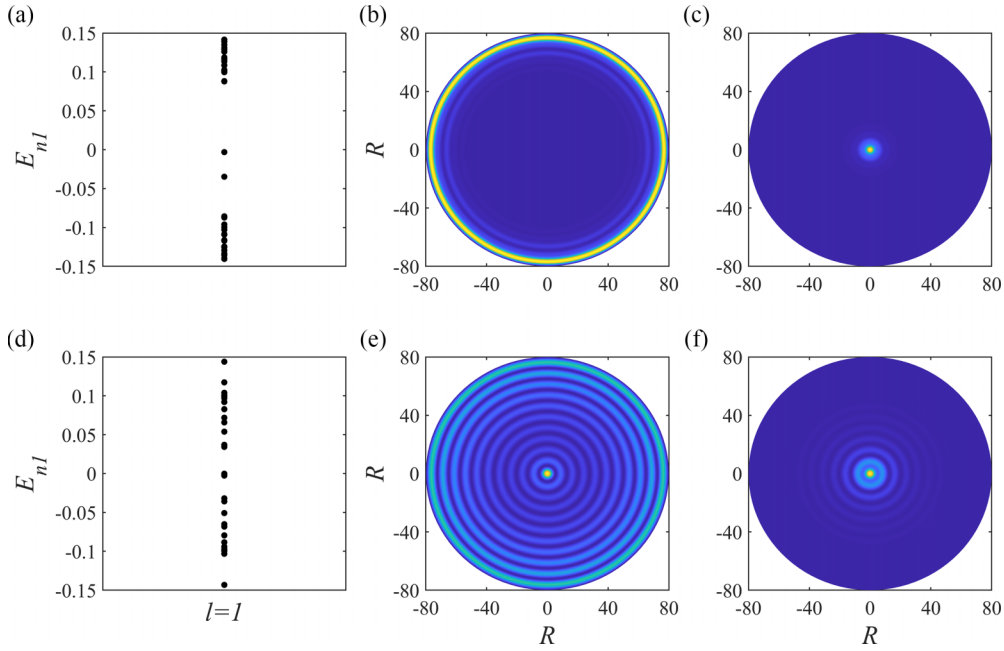

FIG. 3. (a), (d) The quasiparticle energy and density of possibility of (b), (e) EM and (c), (f) VCM at $l = 1$ channel under positive ZF $B_z = 0.2$ with (a)–(c) $\alpha = 0.5$ and (d)–(f) $\alpha = 0.1$.

the quest to observe non-Abelian statistics of quasiparticles within this system. The slopes of the EMs exhibit an interesting behavior: they have opposite directions for two opposite ZFs. This behavior signifies that electrons can only move in a clockwise or anticlockwise direction at the system's edge, indicating the occurrence of the quantum anomalous Hall effect [32,33].

C. Vortex core modes with zero energy

In the trivial parameter region $B_z^2 < \Delta_s^2 + \mu^2 = 0.1$, there consistently exists an energy gap within the system, as illustrated in Fig. 4. However, it is worth noting that this gap does not precisely close at $B_z = 0.1$ due to the finite-size effect mentioned earlier. It is understandable that the gap closure occurs earlier under negative ZF than under positive ZF, resulting in distinct oscillation patterns. For cases of weak SOC, the gap expands, in stark contrast to the behavior observed in the topological parameter region. Simultaneously, the finite-size effect becomes more pronounced. Surprisingly, an unexpected zero-energy state emerges within the trivial parameter region that, under the influence of negative ZF, should have remained fully gapped. Remarkably, this zero-energy state is identified as VCMs possessing an unexpected zero-energy feature, as depicted in Fig. 5. To provide an explanation for this phenomenon, we consider a scenario in which both the strength of the SOC and the off-diagonal superconducting order parameter are exceedingly weak, such that $\alpha = 0$ and $(\Delta_l)_{i\neq j} = 0$. Under these conditions, the BdG matrix can be effectively simplified into a block-diagonal form, leading to a condition for the existence of zero-energy states given by

$$B_z = \frac{a_{1j}^2 - a_{0j}^2}{2R^2} - \sqrt{\left(\frac{a_{1j}^2 + a_{0j}^2}{2R^2}\right)^2 + \Delta_0^2}. \tag{5}$$

The maximum negative value of B_z occurs in the smallest $j = 1$ case, where $B_z > -\Delta_0$. When the separation between two adjacent vortices significantly exceeds the coherence length,

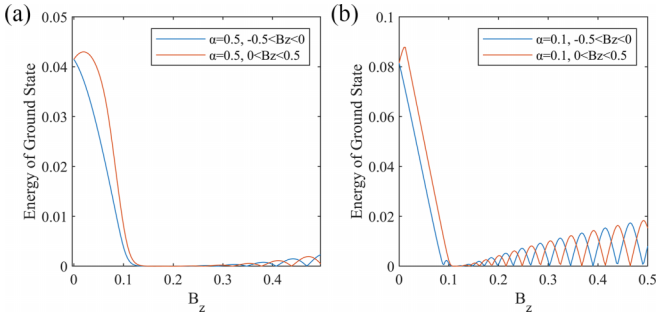

FIG. 4. Evolution of energy of the ground state at $l = 0$ channel with ZF $0.5 > |B_z| > 0$. Two interlaced oscillation patterns are formed in the topological parameter region $B_z^2 > \Delta_s^2 + \mu^2$. A large gap exists in the trivial parameter region $B_z^2 < \Delta_s^2 + \mu^2$.

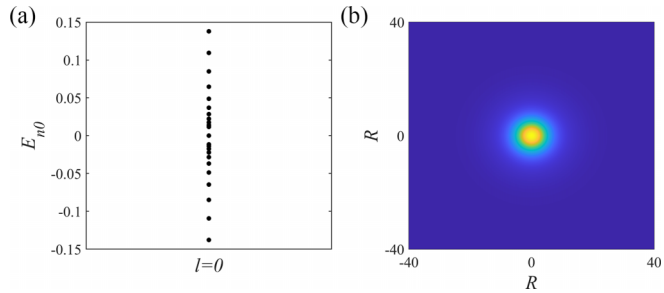

FIG. 5. The quasiparticle energy and density of possibility of zero-energy mode at $l = 0$ channel with $\alpha = 0.1$ and $B_z = -0.089$.

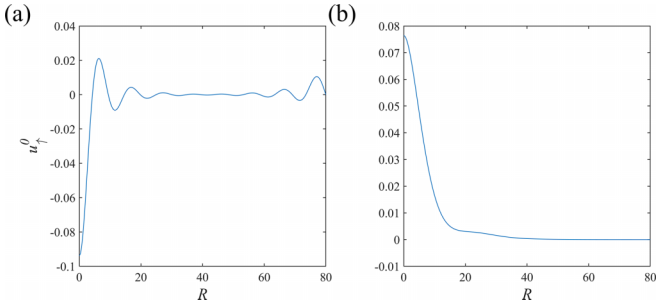

FIG. 6. The wave function of MZM with $\alpha = 0.5$ and $B_z = -0.2$ and zero-energy VCM with $\alpha = 0.1$ and $B_z = -0.089$.

that is, when $2R \gg \xi$, the phenomenon of penetration can be safely disregarded. In this regime, not only do the CdGMMs possess zero energy, but the VCMs can also exhibit zero energy due to the finite-size effect. As demonstrated in Fig. 6, the oscillation pattern disappears in VCMs, presenting a feasible method for distinguishing between MZMs and VCMs in experimental observations.

IV. DISCUSSION AND CONCLUSION

Among the subtle difference between these different modes, we primarily highlight two novel effects: the off-centered effect of MZMs and the penetration effect of VCMs. We contend that a zero-energy mode, whether off-centered or centered, may or may not be a MZM. Based on our comprehensive study, we propose four key requirements to mitigate the interference from trivial bound states in experiment. Weak magnetic field: It is imperative that the strength of the magnetic field remains substantially smaller than the upper critical field, denoted as $H \ll H_{c2}$. This condition ensures that the vortex cores are sufficiently small and the separation between adjacent vortices is adequately large. Strong SOC: A strong SOC is essential to suppress both the off-centered effect and the penetration effect, thus enabling clearer observations of nontrivial modes. Detection of nontrivial EMs: Experimentally, the presence of nontrivial edge modes should be unequivocally observed by applying a local magnetic field. Gradually decaying interference fringes: To further confirm the presence of nontrivial modes and distinguish them from trivial ones, one should look for the appearance of interference fringes that gradually decay with increasing distance from the vortex core center. By satisfying these four requirements, researchers can significantly enhance the reliability of their experimental observations and gain deeper insights into the fascinating world of topological superconductivity.

Here we discuss briefly the effects of SOC, superconducting order parameter, and impurity for these bound states. In general, the wave function of the bound state can be written as $\psi(r) \sim \exp[-\int \Delta(r)dr/\hbar v_F]J_l(ar)$. The Fermi velocity is related to the strength of SOC as $v_F = \hbar k_F/m - \alpha\hbar k_F$ in our case. One can see that a more extended oscillatory pattern will be caused when the SOC or superconducting order parameter decreases. With impurity, the topological nontrivial MZM is robust enough in the vortex based on particle-hole symmetry. A local small perturbation cannot destroy this symmetry or shift the nondegenerate zero-energy MZM to a finite energy that must emerge simultaneously with another negative-energy state. Meanwhile, the unprotected VCM appearing at the trivial region still survives under weak impurity potential but is destroyed under strong impurity scattering. Besides, such strong impurity potential could push the trivial CdGMMs to zero energy with zero charge to imitate the spectroscopic signatures of MZMs [24].

In summary, our study has demonstrated that a vortex within a topological superconducting heterostructure has the capability to trap several distinct types of modes, including MZMs, CdGMMs, VCMs, and EMs. The characteristics of these modes exhibit subtleties contingent on the precise tuning of various parameters, such as the direction of the ZF and the strength of the Rashba SOC, and others. Our investigations have placed important constraints on the experimental verification of MZMs, shedding light on the intricate nature of these exotic quasiparticle states.

ACKNOWLEDGMENTS

This work was financially supported by the National Key R&D Program of China (Grants No. 2022YFA1403200, No. 2017YFA0303201), National Natural Science Foundation of China (Grants No. 92265104, No. 12022413, No. 11674331), the "Strategic Priority Research Program (B)" of the Chinese Academy of Sciences (Grant No. XDB33030100), the Basic Research Program of the Chinese Academy of Sciences Based on Major Scientific Infrastructures (Grant No. JZHKYPT-2021-08), the CASHIPS Director's Fund (Grant No. BJPY2023A09), the Major Basic Program of the Natural Science Foundation of Shandong Province (Grant No. ZR2021ZD01), and the China Postdoctoral Science Foundation (Grant No. 2023M731615). A portion of this work was supported by the High Magnetic Field Laboratory of Anhui Province, China.

[1] F. Wilczek, Nat. Phys. **5**, 614 (2009).
[2] C. W. J. Beenakker, Annu. Rev. Condens. Matter Phys. **4**, 113 (2013).
[3] A. Yu. Kitaev, Ann. Phys. **303**, 2 (2003).
[4] T. M. Rice and M. Sigrist, J. Phys.: Condens. Matter **7**, L643 (1995).
[5] E. Majorana, Nuovo Cim. **14**, 171 (1937).
[6] G. Moore and N. Read, Nucl. Phys. B **360**, 362 (1991).
[7] L. Fu and C. L. Kane, Phys. Rev. Lett. **100**, 096407 (2008).
[8] V. Mourik, K. Zuo, S. M. Frolov, S. R. Plissard, E. P. A. M. Bakkers, and L. P. Kouwenhoven, Science **336**, 1003 (2012).
[9] L. P. Rokhinson, X. Liu, and J. K. Furdyna, Nat. Phys. **8**, 795 (2012).
[10] J.-P. Xu, M.-X. Wang, Z. L. Liu, J.-F. Ge, X. Yang, C. Liu, Z. A. Xu, D. Guan, C. L. Gao, D. Qian, Y. Liu, Q.-H. Wang, F.-C. Zhang, Q.-K. Xue, and J.-F. Jia, Phys. Rev. Lett. **114**, 017001 (2015).

[11] H.-H. Sun, K.-W. Zhang, L.-H. Hu, C. Li, G.-Y. Wang, H.-Y. Ma, Z.-A. Xu, C.-L. Gao, D.-D. Guan, Y.-Y. Li, C. Liu, D. Qian, Y. Zhou, L. Fu, S.-C. Li, F.-C. Zhang, and J.-F. Jia, Phys. Rev. Lett. **116**, 257003 (2016).
[12] T. H. Hsieh, H. Lin, J. Liu, W. Duan, A. Bansil, and L. Fu, Nat. Commun. **3**, 982 (2012).
[13] Y. Tanaka, Z. Ren, T. Sato, K. Nakayama, S. Souma, T. Takahashi, K. Segawa, and Y. Ando, Nat. Phys. **8**, 800 (2012).
[14] M. Novak, S. Sasaki, M. Kriener, K. Segawa, and Y. Ando, Phys. Rev. B **88**, 140502(R) (2013).
[15] A. S. Erickson, J.-H. Chu, M. F. Toney, T. H. Geballe, and I. R. Fisher, Phys. Rev. B **79**, 024520 (2009).
[16] P. Hosur, P. Ghaemi, R. S. K. Mong, and A. Vishwanath, Phys. Rev. Lett. **107**, 097001 (2011).
[17] J. D. Sau, R. M. Lutchyn, S. Tewari, and S. Das Sarma, Phys. Rev. Lett. **104**, 040502 (2010).
[18] T. Machida, Y. Sun, S. Pyon, S. Takeda, Y. Kohsaka, T. Hanaguri, T. Sasagawa, and T. Tamegai, Nat. Mater. **18**, 811 (2019).
[19] Y. Yuan, J. Pan, X. Wang, Y. Fang, C. Song, L. Wang, K. He, X. Ma, H. Zhang, F. Huang, W. Li, and Q.-K. Xue, Nat. Phys. **15**, 1046 (2019).
[20] C. Caroli, P. G. D. Gennes, and J. Matricon, Phys. Lett. **9**, 307 (1964).
[21] M. Chen, X. Chen, H. Yang, Z. Du, X. Zhu, E. Wang, and H.-H. Wen, Nat. Commun. **9**, 970 (2018).
[22] H. Pan and S. Das Sarma, Phys. Rev. Res. **2**, 013377 (2020).
[23] D. Wang, L. Kong, P. Fan, H. Chen, S. Zhu, W. Liu, L. Cao, Y. Sun, S. Du, J. Schneeloch, R. Zhong, G. Gu, L. Fu, H. Ding, and H.-J. Gao, Science **362**, 333 (2018).
[24] B. S. de Mendonça, A. L. R. Manesco, N. Sandler, and L. G. G. V. Dias da Silva, Phys. Rev. B **107**, 184509 (2023).
[25] Y. Jiang, M. Ermolaev, S. Moon, G. Kipshidze, G. Belenky, S. Svensson, M. Ozerov, D. Smirnov, Z. Jiang, and S. Suchalkin, Phys. Rev. B **108**, L121201 (2023).
[26] M. Z. Hasan and C. L. Kane, Rev. Mod. Phys. **82**, 3045 (2010).
[27] M. Kohda, T. Okayasu, and J. Nitta, Sci. Rep. **9**, 1909 (2019).
[28] J. D. Sau, S. Tewari, R. M. Lutchyn, T. D. Stanescu, and S. Das Sarma, Phys. Rev. B **82**, 214509 (2010).
[29] L. Mao and C. Zhang, Phys. Rev. B **82**, 174506 (2010).
[30] X. Wu, S. B. Chung, C. Liu, and E.-A. Kim, Phys. Rev. Res. **3**, 013066 (2021).
[31] B. Zhou, H.-Z. Lu, R.-L. Chu, S.-Q. Shen, and Q. Niu, Phys. Rev. Lett. **101**, 246807 (2008).
[32] C.-X. Liu, S.-C. Zhang, and X.-L. Qi, Annu. Rev. Condens. Matter Phys. **7**, 301 (2016).
[33] C.-Z. Chang, J. Zhang, X. Feng, J. Shen, Z. Zhang, M. Guo, K. Li, Y. Ou, P. Wei, L.-L. Wang, Z.-Q. Ji, Y. Feng, S. Ji, X. Chen, J. Jia, X. Dai, Z. Fang, S.-C. Zhang, K. He, Y. Wang *et al.*, Science **340**, 167 (2013).